Subwavelength Focusing of Light From a Metallic Slit Surrounded by Grooves with Chirped Period

Jaewoong Yoon, Kiyoung Choi, Seok Ho Song*, and Gwansu Lee

Microoptics Lab., Dept. of Physics, Hanyang University, Seoul 133-791, KOREA

Extraordinary phenomena related to the transmission of light via metallic films with subwavelength holes and grooves are known to be due to resonant excitation and interference of surface waves. These waves make various surface structures to have optically effective responses. Further, a related study subject involves the control of light transmitted from a single hole or slit by surrounding it with diffractive structures. This paper reports on the effects of controlling light with a periodic groove structure with Fresnel-type chirping. In Fresnel-type chirping, diffracted surface waves are coherently converged into a focus, and it is designed considering the conditions of constructive interference and angular spectrum optimization under the assumption that the surface waves are composite diffracted evanescent waves with a well-defined in-plane wavenumber. The focusing ability of the chirped periodic structures is confirmed experimentally by two-beam attenuated total reflection coupling. Critical factors for achieving subwavelength foci and bounds on size of focal spots are discussed in terms of the simulation, which uses the FDTD algorithm.

OCIS codes : 240.0240, 240.6680, 240.6690

I. INTRODUCTION

Subwavelength periodic structures on metallic films exhibit many extraordinary phenomena in certain spectral ranges: for instance, the enhanced transmission of light through subwavelength hole arrays [1,2], and the beaming of light from a single subwavelength hole or slit flanked by periodic surface corrugations [3]. It is evident that the enhancement of the transmission is due to cavity resonance in grooves or holes [4] and the constructive interference of composite diffracted evanescent waves (CDEWs) by each groove or hole, rather than by surface plasmon-polaritons [5,6]. Recently, it was reported that these phenomena can be generally attributed to surface modes named 'spoof' surface plasmon-polaritons, whose propagation properties are determined by the geometry of the metallic surface [7,8]. In any case, the resonant excitation of a surface wave from a subwavelength aperture means that the optical field extends over an area much larger than that of the aperture. This extended area likely acts as an effective optical aperture. Various photonic structures can be placed around the aperture, by which properties of the transmitted light can be controlled. Garcia-Vidal et al. reported that transmitting light through a single aperture surrounded by a finite array of grooves with a fixed period focuses the light [9].

They obtained universal curves for defining the foci as functions of the number of grooves, N. As N increases, the overall optical transmission is enhanced, but the foci become more elongated in both the longitudinal and transverse directions. It can be pointed out that the angular spectra of the fields re-emitted from CDEWs by each of the N grooves are identical, leading to the focal elongation with N2 dependence.

In this paper, we report the effect of chirping in groove periods on light transmission from a metallic slit. Chirping in groove periods was applied to form a subwavelength focus in the near-field region via constructive interference. Experimental verification of the effect on near-field focusing was performed by two-beam attenuated total reflection (ATR) measurement. Finally, we confirmed agreement with the experimental results and showed how tight foci can be made by the chirped groove structure using finite difference time domain (FDTD) simulation. The location and geometry of the subwavelength focal spot was also demonstrated numerically.

II. METHOD OF CHIRPING IN THE GROOVE PERIODS

In this section we describe the method for using chirping for focusing light in the optical near field. (By 'optical

near field,' we mean a few to a few tens of microns, rather than the subwavelength vicinity of the surface. The region can be thought of as intermediate between the optical near- and far-fields regorously.) To determine appropriate positions for the grooves, a condition for the constructive interference of radiation from different grooves is considered. A schematic is given in Fig. 1 (a). The metallic film is assumed to be free-standing in a vacuum. Light of wavelength λ_0 is shone on the left side of the film, transmitted through the hole, and then diffracted into radiative modes by the grooves. If we assign the position of the pth groove such that the total phase change from the hole to the focal point via that groove satisfies $\phi_r(p) = \phi_r(0) + 2\pi p$ (where p is an integer not less than 0), the radiated optical field from each groove interferes constructively, that is, the incident light is diffracted so as to form a focus. The phase change from the pth groove to the focal point, $\phi_R(p)$, is given by 2π times of relative optical path length to the wavelength. On the other hand, to determine the phase change from the hole to the pth groove, $\phi_E(p)$, the spatial amplitude of the transmitted field should be known in advance. It is experimentally well-established in the recent paper by H. J. Lezec et al. that the optical response of an opaque film (metallic or otherwise) with subwavelength features is explained successfully for a variety of structures by assuming a composite diffracted evanescent wave (CDEW), with a spatial amplitude function given by
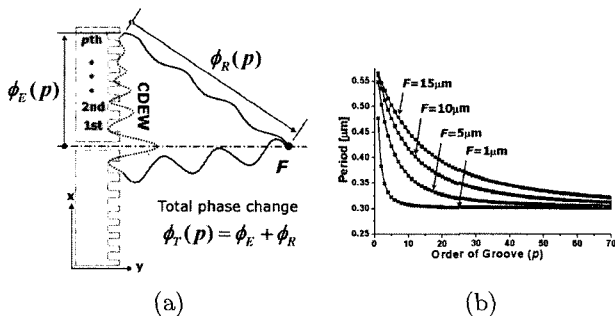

(a)   (b)

FIG. 1. (a) Schematic for determining the position of the pth groove. F indicates focal length. $\phi_E(p)$ and $\phi_R(p)$ are the phase change of composite diffracted evanescent wave (CDEW) from the hole to the pth groove and that of radiation from the pth groove to the focal point, respectively. (b) The local periods of grooves for different focal lengths given by Eq. (1) when the wavelength of incident light is 0.6328 μm and $n_E = 1.1$. The square symbols indicate the periods calculated by the constructive interference condition, and the lines represent the periods calculated by angular spectrum optimization, the exact definition of which is in the text. The maximum difference between the periods by the two methods is found in case for $F=1$ μm, and the difference is about 0.4% of the corresponding period. Thus, it can be regarded that the two methods produce identical results.

$C(x)\cos\left(n_E k_0 x + \pi/2\right)$, as a main channel [5]. Therefore, an effective choice for $\phi_E(p)$ would be $n_E k_0 x(p) + \pi/2$, where $x(p)$ is the position of the pth groove. Then, the position of pth groove can be calculated by the relation $n_E x(p) + [x(p)^2 + f^2]^{1/2} + \lambda_0/2 = f + p\lambda_0$, where F is focal length. (Note that the additional phase shift is π, not $\pi/2$, because there are two diffraction processes: the one of diffraction from the hole-transmitted wave to the CDEW and the one from the CDEW to radiation.) The relation results in following expression

$$x(p) = \frac{n_E[F+(P-0.5)\lambda_0]}{n_E^2-1} - \left(\left\{\frac{n_E[F+(P-0.5)\lambda_0]}{n_E^2-1}\right\}^2 \right.$$
$$\left. - \frac{(p-0.5)\lambda_0[2F+(p-0.5)\lambda_0]}{n_E^2-1}\right)^{1/2} \quad (1)$$

The limiting behavior of $x(p)$ is interesting. Near the hole, $x(2)-x(1) \cdot \lambda_0/n_E$ when $\lambda_0 \ll F$. This value can be thought of as the local period of the grooves at the center of the structure. In this case, the corresponding local grating vector is $K(0) = n_E k_0$, by which a single component of the evanescent wave with surface wavevector $k_x = n_E k_0$ is diffracted into a radiative mode propagating along the surface normal direction ($k_x = n_E k_0 - K(0) = 0$ and $k_y = k_0$). On the other hand, far from the hole ($x(p) \gg F$), we can approximate Eq. (1) by $x(\lambda_0 \gg F) = p\lambda_0/(n_E + 1)$. Hence, the corresponding local period - the difference between the positions of the pth and $(p+1)$th groove - approaches $\Lambda(x \gg F) = \lambda_0/(n_E + 1)$. This gives a local grating vector of $K(x \gg F) = (n_E + 1)k_0$. The magnitude of this vector gives a partial planewave that propagates anti-parallel to the CDEW in a diffracted mode, because the surface and surface normal wavevector of the diffracted mode is given by $k_x = n_E k_0 - K(x \gg F) = -k_0$ and $k_y = 0$, respectively. Fig. 1 (b) shows the local periods of the grooves as functions of focal lengths. The square symbol indicates the period defined by $\Lambda(p) = x(p) - x(p-1)$, and the line represents the local period, $\Lambda'(p)$, calculated by the equation $2\pi/\Lambda'(p)-n_E k_0 = k_0 X(p)/[X(p)^2 + F^2]^{1/2}$, where $X(p) \equiv [x(p)+x(p-1)]/2$ is the average position of the pth and $(p+1)$th grooves. The equation for $\Lambda'(p)$ is composed so that diffracted mode at $X(p)$ directs the focal point without regard for the phase of the diffracted wave at the focal point; we thus refer to this method as 'angular spectrum optimization'. Fig. 1 (b) shows that $\Lambda(p)$ and $\Lambda'(p)$ agree well with each other. The consistency of the periods given by the condition of constructive interference and those by angular spectrum optimization means that when the groove positions are as given by Eq. (1), the film diffracts the CDEW so that the phase front converges circularly into the focal point as in a cylindrical wave, because the partial diffracted waves from all grooves would have the same phase and converge at the focal point. Note that the only difference between this type of chirped groove arrangement and

a cylindrical Fresnel lens is scale. This results from the assumption that the effective index of the CDEW is uniform along the surface. If we take the effective index of the CDEW (n_E) to be 0, $x(p)$ is exactly the same as for the cylindrical Fresnel lens.

III. VERIFICATION OF THE FOCUSING ABILITY BY TWO-BEAM ATR EXPERIMENT

To confirm the focusing ability of a film with chirped grooves whose positions are given by Eq. (1), we performed a two-beam ATR experiment. The schematic for the experiment is depicted in Fig. 2. TM-polarized light from a He-Ne laser ($\lambda_0 = 632.8$ nm) was split into two parallel beams by the beam splitter and mirror (M1). The upper beam was refracted directly into one side of the prism (FD10 glass, n=1.8294), and the lower was reflected by the mirror (M2) and then refracted into another side of the prism.

The two beams illuminate the sample on the diagonal face of the prism as two counter-propagating, evanescent waves when the internal incident angle (Θ) is larger than the critical angle (33.1° in this case). Index-matching fluid with a refractive index of 1.8 was used for the sample attachment. The microscope image showed the light intensity distribution from the chirped groove structure at the object plane. By scanning the object plane (or the microscope) along the direction normal to the
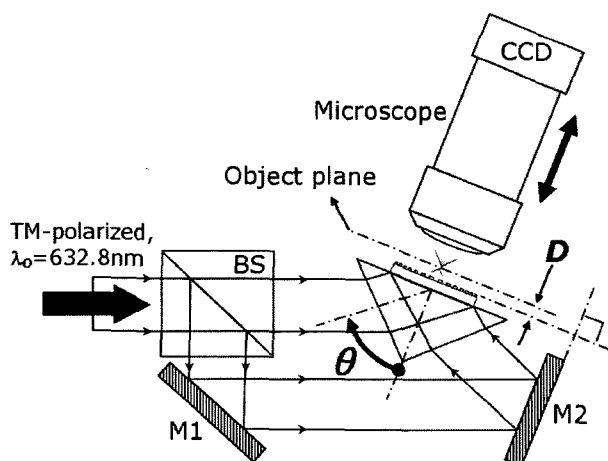
sample face, features of the intensity distribution could be directly observed, including whether the emitted light forms a focus and where the focus forms. This type of ATR-coupling device is easily made and is known to provide a well-defined, controllable effective index of evanescent waves by tuning the internal incident angle. The effective index of evanescent wave is given by $n_E = n_{prism}$, and the precision of the effective index is determined directly by the precision of the internal incident angle, and is given by $\Delta n_E = n_{prism} \cos\theta \Delta\theta$. In our case, the angular precision was about 10^{-3} radian, giving a precision for the effective index of about 10^{-3}. PMMA was used for the groove structure to ensure that enough incident fields were coupled into evanescent waves. Groove structures were fabricated by electron-beam lithography (JSM35-CF Scanning electron microscope, JEOL Ltd.) in a 83-nm PMMA film (2% PMMA 950k, spin coated at 5000 rpm) on a 50-nm Au film, as shown in Fig. 3. FD10 glass was used for the substrate. Though the grooves were not made in a metal layer, the PMMA grooves were optically shallow enough so as not to excite resonant or guiding modes for TM-polarized light and, therefore, affected the system as scattering objects for the evanescent waves. Thus, if we are concerned only with the spatial distribution of emitted light (and not its efficiency), this type of dielectric structure would be sufficient to determine whether the chirping method creates the desired focus. The fabricated sample was composed of nine patterns; each pattern covered a 30 µm × 30 µm area and was designed to exhibit a different focal length. In Fig. 3 (a), the focal lengths are, from right to left, 10, 20, and 30 µm in the top row, 40, 50, and 60 µm in the second row, and 70, 80, and 90 µm in the bottom row. The local periods range from 570nm

FIG. 2. Schematic of two-beam attenuated total reflection (ATR) apparatus for observing the focused emission of a single component evanescent wave. θ and D are the internal incident angle and the surface normal distance from the sample surface to the object plane of microscope, respectively. Two mirrors, M1 and M2, are aligned so that the incident angles of the two beams are the same. D is adjusted by a motorized translation stage with 0.25 µm resolution. By observing microscope images according to D, the length, depth, and horizontal intensity profile of the focus can be determined.
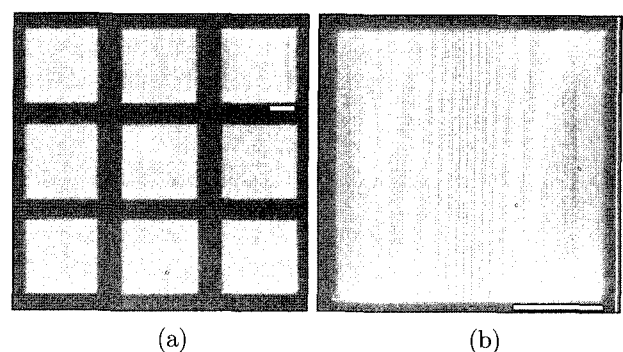

(a)   (b)

FIG. 3. Scanning electron micrograph of the fabricated sample. Grooves are written in the PMMA layer with a thickness of 100 nm by electron beam lithography. FD10 glass is used for the substrate. (a) depicts the full sample array. Each sample has a different focal length. The designed focal lengths are 10 ~ 90 µm from the right-top to the left-bottom corners in increments of 10 µm. (b) shows the pattern of the 10 µm focal length. Two white bars represent 10 µm.

at the center of each pattern to 300 nm near the margins. Microscope images of the light emitted from the top row (F=10, 20, and 30 μm) taken at four different distances (D) between the sample surface and the object plane are shown in Fig. 4 (a). The images show that the emitted light forms a focus at the intended position. For more exact evaluation, horizontal profiles at the center of each row were taken from D=0 μm to D=110 μm in 1 μm intervals. Fig. 4 (b), (c), and (d) show intensity plots of the horizontal profiles for the top, middle, and bottom rows, respectively. The focal lengths are marked below the positions of each pattern. The emitted light formed a focus at the exact position expected. The differences between the observed and intended focal lengths were less than 3 μm, which can be attributed to the uncertainty in defining the position of the D=0 plane. The numerical aperture of the objective lens used for imaging was 0.25, and the corresponding depth of focus was 6.4 μm. We cannot distinguish the in-focus and out-of-focus images over a change in position smaller than about half of the focal depth. Therefore, the observed
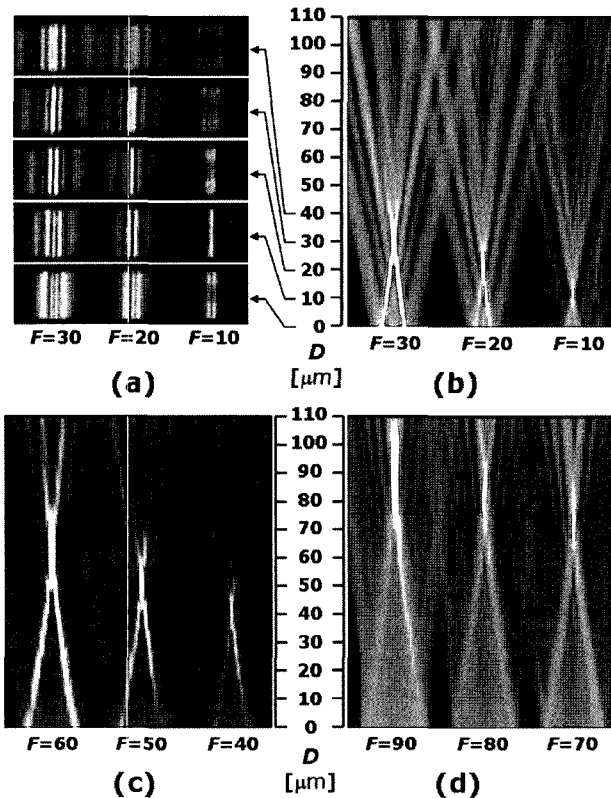
positions of the foci show good agreement with the intended positions within reasonable experimental error. Taking vertical profiles at the center of each pattern and the horizontal profile at the focal plane proved to be helpful for determining the quality of the focus (that is, its depth and size). These profiles are given in Fig. 5. The intended focal points are all in the focal depths in Fig. 5 (a), (b), and (c); this means that the actual locations of the foci correspond well with the intended ones. Focal depths (FWHM) were measured to be 13, 15, 13, 14, 16, 23, 31, 33, and 40 μm from F=10 μm to F=90 μm by 10 μm interval. This suggests that the focal depth is constant for focal lengths smaller than 40 μm, that it increases linearly for focal lengths larger than 50 μm approximately. The horizontal width of the focus shown in Fig. 5 (d) was 2 μm for the focal length of 10 μm, and increased gradually with focal lengths to 4 μm for a focal length of 90 μm. For the condition of surface plasmon resonance (internal incident angle of 41.67°, $n_E = 1.216$), the overall distribution of intensity for the transmitted light was the same as for $n_E = 1.1$. The total transmittance of each pattern obtained by summation of CCD output values over a horizontal cut-line at the focal position, however, was enhanced about 25 times when $n_E = 1.1$. This value of enhancement agrees well with that given by rigorous coupled wave analysis based simulation. The enhancement factors from the simulation ranged from 24 (for the F=90 mm pattern) to 30 (the F=20 mm pattern). Note that this degree of enhancement is not the same as the hole-transmitted case in its mechanism, though it is common for the efficient mediation of surface waves to enhance

FIG. 4. (a) Microscope images of the emitted light according to D=0, 10, 20, 30 and 40 μm from below. (b), (c), and (d) are intensity plots of cross-sectional profiles taken from the horizontal line at the center of the microscope images of each row. One-hundred and eleven images in 1 μm increments were used (D=0, 1,..., 110 μm). The internal incident angle is 36.96° and corresponds to the effective index of n_E=1.1.
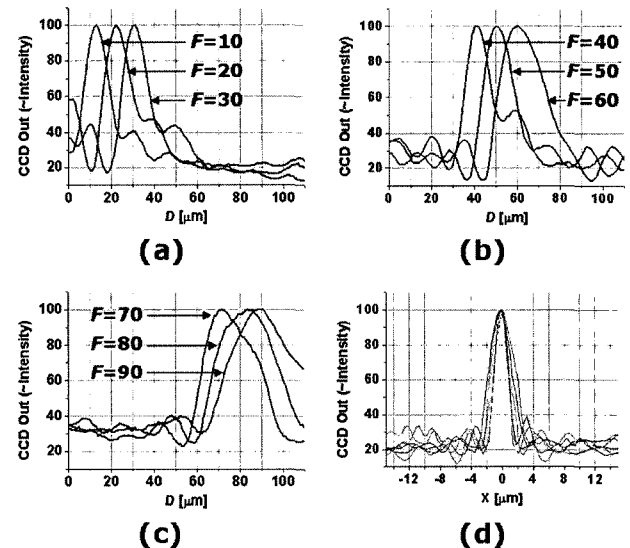

FIG. 5. (a), (b), and (c) are plots of surface normal intensity profiles at the center of each pattern. (d) shows horizontal profiles of the foci. The beam width (FWHM) is about 2 μm for F=10 μm and 4 μm for F=90 μm.

transmission. The field enhancement for ATR coupling results from the fact that the surface plasmon energy velocity is slower than the surface projection of the energy velocity of incident planewave. On the other hand, transmission enhancement for the hole-transmitted case is due to Fabry-Perot resonance at the hole and groove cavity resonance [4].

The experimental results showed that the chirping method can be used well single component of plane evanescent wave to be emitted with focus located at the desired position. In case of CDEW (not single components of evanescent waves), it is expected that the actual focal lengths agree well with the intended ones as shown in the two-beam ATR experiment, because the surface wavevector of a CDEW transmitted through a hole is well-defined [5]. However, the width and depth of the focus may not be consistent with the experimental results: The amplitude of the evanescent wave coupled by ATR is uniform over the chirped groove structure; however, CDEWs have a $1/x$ dependence on its amplitude. Moreover, radiation by the grooves results in additional decay with exponential dependence on the number of grooves experienced. Therefore, the effective numerical aperture - the main factor that determines the focal width and depth - is limited by a value determined by the scattering amplitude per groove. As a result, the applicability of the results obtained by the two-beam ATR experiment to focusing light from a hole is restricted.

IV. NUMERICAL SUTDY ON THE FOCUSING OF THE TRANSMITTED LIGHT FROM A SLIT

It was confirmed experimentally in the previous section that a film with groove distribution given by Eq. (1) can be used to emit radiation with a focus at a desired position from an evanescent surface wave whose surface wavevector is well-defined. In this section, we discuss our numerical investigation that uses a 2-dimensional FDTD algorithm of how the focus can be formed tightly and efficiently by the chirping method for the case of single slit transmission. In the simulations, we assumed a vacuum wavelength $\lambda_0 = 0.6328$ µm, slit and groove widths of 100 nm, and the Ag film thickness of 300 nm (plasma and collision frequency of 1.14×10^{16} and 1.26×10^{14} radian/s) [10].

We first found a condition for unchirped grooves on both sides of the Ag film that maximized total transmission with well-collimated output. It had already been established that the total transmission efficiency of a slit flanked by periodic grooves is nearly independent of the output grooves but dependent on the geometrical properties of the grooves on the input surface (width, depth, and periods). The transmission is maximized at the condition of resonant excitation for surface waves with anti-resonance in the reflected wave [4]. The spatial

distribution of the transmitted light is known to be determined, however, by geometry of the grooves on the output surface [9]. Accordingly, we found in advance the period of input grooves at fixed depth (50 nm) that maximizes transmission, and then found the depth of the output grooves that gives the best collimation. Maximum transmission was obtained with the period $\Lambda = \lambda_0/1.18 = 0.5363$ µm. At this period, emitted light was well-collimated for 40-nm grooves on the output surface, as shown at the "not-chirped" case in Fig. 6. The intensity at the center of the beam on the plane 20 µm away from the upper Ag surface was about 30% of the intensity of incident light. As chirping was applied to output grooves, the emitted light forms a focus at the intended position, as shown in Fig. 6. The groove positions were determined by Eq. (1) with $n_E = 1.18$, the same value as that determined from the relative magnitude of the grating vector for input grooves to the vacuum wavevector of incident light $(2\pi/\lambda_0)$. Note that the value 1.18 may be different from the exact value of CDEW transmitted via the slit. One reason for this is that the dependences of slit geometry on CDEWs have not yet been established. The value 1.1 for the effective index for CDEWs which had been given by phenomenological fitting in the ref. 5 has also not yet been explained. The total transmission is determined by the constructive interference of the CDEWs via the input grooves at the slit, and the focusing is determined by the CDEWs from the slit on the output surface. Although the widths of the slit and the grooves are the same here, their depths are different. Therefore, the effective indices of CDEWs via the input grooves and those from the slit may be different. Another factor is that the maximum transmission requires anti-resonance in the reflected wave on the input surface. In the reflection anomaly from a metallic grating (known
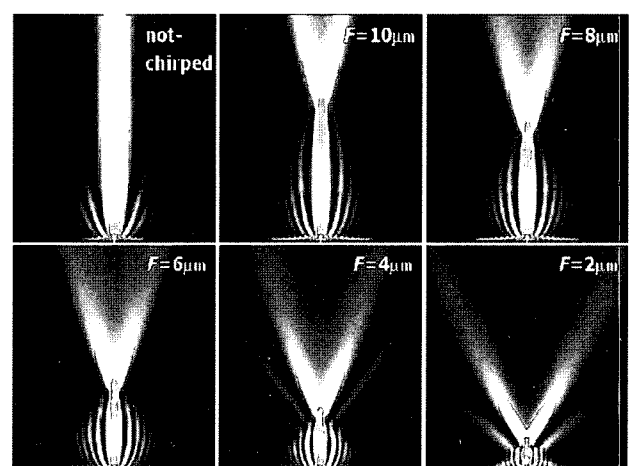

FIG. 6. Distribution of time-averaged magnitude of Poynting vector (FDTD simulation). The designed focal lengths are indicated on the right-top corner of each figure. The widths of the central hole and grooves are all 100 nm.

as the Wood anomaly) which appears when surface waves are excited at resonance, the positions of the resonance and anti-resonance of reflection in the angular spectrum are slightly detuned from the exact position of the wave-vector of the surface wave [11,12]. Fig. 6 gives the color, which ranges from black (0) to white (intensities greater than $3I_0$, where I_0 is intensity of the incident light). The values represent magnitudes of the Poynting vectors averaged over the half-temporal period of the incident light. Interference fringes between the hole and the focus can be seen in all cases. This indicates that the light emitted by the grooves has a phase front like that of a cylindrical wave centered at the focal point, because this kind of interference pattern is created when the two cylindrical waves with different source positions interfere. It can be regarded in these cases that one cylindrical wave is transmitted directly from the hole, and the other is emitted coherently by the grooves. It is notable that there exists an optimal output surface groove depth for creating a focus efficiently. In this case, the optimum depth is 40 nm. The existence of an optimal depth can be explained by the two facts: the size of the effective optical aperture which contributes to the formation of a focus is tuned by the depth of the groove, and the area in which most of the trans-mitted field exists at the output surface has finite size. At depths greater than the optimal, the number of grooves that contribute effectively to scatter the surface wave into the radiation decreases, because the field decays faster along the surface; the effective numerical aper-ture also shrinks. This results in a looser focus. If the grooves are shallower, however, a directly transmitted wave with divergent directionality is more dominant than the waves scattered by the grooves. Moreover, the effective numerical aperture is limited by the size of the area in which most of the field is concentrated. Accor-ding to our simulation, depths of 30 nm and 50 nm give much weaker foci. With focal lengths of 4 μm, the intensi-ties at the foci are less than 60% of those produced by the optimum groove depth of 40 nm. For focal lengths larger than 8 μm, this effect becomes more dramatic, and the grooves produce no distinguishable focus. The longitudinal and horizontal profiles of the intensity dist-ributions for the optimum depth (40 nm) are depicted in Figs. 7 (a) and (b). The profiles show that smaller focal lengths produce a tighter focus. As shown in the longitudinal profiles, all focal points are shifted from the intended positions to ones less distant from the film. The deviations from the intended focal lengths are 18.6%, on average. This shift can be attributed to inexact estimation of the effective index (n_E) of the CDEW by the central slit. There may be several methods, however, for finding the exact effective index. One simple way is to compare the chirping ratios between two different effective indices. If we expand Eq. (1) by powers of $\lambda_0 p/F$, the local period can be written as

$$\Lambda(p) = x(p) - x(p-1) = \frac{\lambda_0}{n_E} - \frac{\lambda_0^2 p}{n_E^3 F} + \frac{\lambda_0^3 p^3}{2n_E^5 F^2} \cdots \qquad (2)$$

For the amplitude of evanescent wave on the output surface decays exponentially in addition to $1/x$ profile along the surface, the dominant contribution for focusing comes from the grooves of the neighbors nearest from the slit. Therefore, the linear chirping ratio with respect to p in Eq. (2), $C^{(1)} = \lambda_0^2/(n_E^3 F)$, can be regarded as the dominant factor in focusing. If the chirping of the groove period is fixed and the exact focal length by the groove structure is known, we can estimate the value of the effective index using the relation $n_E = [\lambda_0^2/C^{(1)}F]$. In the simulation results, $n_E = 1.18 \times [F(\text{designed})/F(\text{real})]^{1/3}$, and $F(\text{designed})/F(\text{real}) = 1\text{-}0.186 = 0.8146$. This gives $n_E = 1.264$. In Figs. 7 (c) and (d), the focal depths and widths are presented in units of the incident wavelength. The focal depths and widths show monotonic increases with focal length. In particular, the focal width for a focal length of 1 μm is less than the diffraction limit (0.5 λ_0). This does not mean that the length rigorously circu-mvents the diffraction limit, however, because the focal point is located in the optical near-field, where the evanescent wave has significant amplitude. Fig. 7 (a) clearly shows that the focus for the case of F=1 μm is located at a position where the evanescently decaying profile from the surface is nonvanishing. As the wave-length of the evanescent wave on the output surface is λ_0/n_E, the limitation for the focal width can be thought to be given by $\lambda_0/(2n_E)$ in the optical near-field of the output surface; the value of the limit is about when $2n_E = 1.264$.
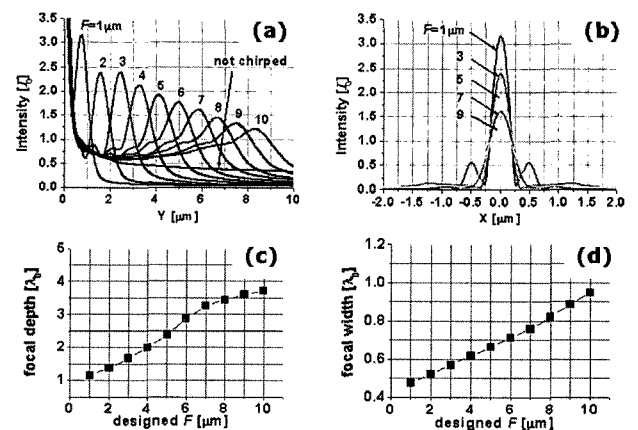

FIG. 7. (a) Longitudinal intensity profiles of the line at the center of the hole and (b) horizontal profile at the focal position in units of incident intensity (I_0). The numbers above (a) and left (b) of each curve indicate the intended focal lengths. Focal depths (c) and widths (d) are obtained by FWHM of well-fitted Gaussian functions.

V. CONCLUSION

Fresnel-type chirping is suggested as a method for transmitting light from a single slit with tight focus. The chirping method considers the constructive interference conditions to determine groove positions, under the assumption that the waves are CDEWs characterized by a well-defined surface wavenumber and a surface wave $\pi/2$ phase shift on the output surface. Correspondence between the chirping method and angular spectrum optimization shows that this type of chirping can function as a cylindrical lens. It is confirmed experimentally by two-beam ATR coupling that the chirping method makes a single component of an evanescent wave form a well-defined focus located at the position intended. Finally, a single slit-transmitted case is simulated using an FDTD algorithm. It can be found that the focusing efficiency is tuned sensitively by the depth of the grooves on the output surface, and that an optimal depth is created by the trade-off between the enlargement of the effective optical aperture and competition of diffracted waves from the grooves with the directly transmitted wave from the central slit. For an incident wavelength of 632.8 nm, the subwavelength focal spot can be achieved using the suggested chirping method when the focal lengths are less than 10 µm, and the size of the focus is confirmed to be limited to $\lambda_0/(2n_E)$. With this type of lens, an incident planewave can be converted into subwavelength spot in a few micron scales. Thus, the apparatus could be used as a compact adapter between the optical near and far fields, and has potential applications including a near-field optical probe generator for microscopy and high-density optical data storage, and a mode relay between two different waveguides. It is worth considering not only Fresnel-type chirping grooves, but also various DOE-like structures which may offer more general ways to control transmitted light via metallic holes. For example, beam shaping or multi-spot generation could be achieved by a CGH analogy of metallic grooves.

*Corresponding Author: shsong@hanyang.ac.kr

REFERENCES

[1] T. W. Ebbesen, H. J. Lezec, H. F. Ghaemi, T. Thio, and P. A. Wolff, "Extraordinary optical transmission through subwavelength hole arrays," Nature, vol. 391, 667-669 (1998).

[2] L. Martin-Moreno, F. J. Garcia-Vidal, H. J. Lezec, K. M. Pellerin, T. Thio, J. B. Pendry, and T. W. Ebbesen, "Theory of extraordinary optical transmission through subwavelength hole arrays," Phys. Rev. Lett., vol. 86, 1114-1117 (2001).

[3] H. J. Lezec, A. Degiron, E. Devaux, R. A. Linke, L. Martin-Moreno, F. J. Garcia-Vidal, and T. W. Ebbesen, "Beaming light from a subwavelength aperture," Science, vol. 297, 820-822 (2002).

[4] F. J. Garcia-Vidal, H. J. Lezec, T. W. Ebbesen, and L. Martin-Moreno, "Multiple paths to enhance optical transmission through a single subwavelength slit," Phys. Rev. Lett., vol. 90, 21391 (2003).

[5] H. J. Lezec and T. Thio, "Diffracted evanescent wave model for enhanced and suppressed optical transmission through subwavelength hole arrays," Opt. Express, vol. 12, 3629-3651 (2004).

[6] J. Yoon, S. H. Song, C.-H. Oh, and P.-S. Kim, "Back-propagating modes of surface polaritons on a cross-negative interface," Opt. Express, vol. 13, 417-427 (2005).

[7] J. B. Pendry, L. Martin-Moreno, and F. J. Garcia-Vidal, "Mimicking surface plasmons with structured surfaces," Science, vol. 305, 847-848 (2004).

[8] A. P. Hibbins, B. R. Evans, and J. R. Sambles, "Experimental verification of designer surface plasmons," Science, vol.308, 670-672 (2005).

[9] F. J. Garcia-Vidal, L. Martin-Moreno, H. J. Lezec, and T. W. Ebbesen, "Focusing light with a single subwavelength aperture flanked by surface corrugations," Appl. Phys. Lett., vol. 83, 4500-4502 (2003).

[10] E. D. Palik, Handbook of Optical Constants of Solids: Volume 1 (Academic Press, 1998).

[11] R. W. Wood, "Anomalous diffraction gratings," Phys. Rev., vol. 48, 928-936 (1935).

[12] U. Fano, "The theory of anomalous diffraction gratings and of quasi-stationary waves on metallic surfaces (Sommerfeld's waves)," J. Opt. Soc. Am., vol. 31, 213-222 (1941).